ChemCatChem

Research Article
doi.org/10.1002/cctc.202500618

Chemistry Europe
European Chemical Societies Publishing

www.chemcatchem.org

Reproducibility in Artificial Photosynthesis: A Case Study on SnO_2/Cu Photocatalysts

Gustavo D. Iga,[a, b] José B. G. Filho,[b] Juliana A. Torres,[a, b] José Lucas Vieira,[a] and Caue Ribeiro*[b]

This study examines how synthesis routes and storage conditions affect the reliability of photocatalytic data for SnO_2/Cu catalysts. Our findings show that nanoparticle stability and photocatalytic performance are significantly influenced by adsorbed ethanol from synthesis—a factor often overlooked in soft-chemistry methods. Ethanol adsorbates show strong stability, resisting standard removal techniques, and directly affecting photocatalytic results. Over two weeks, these adsorbates persisted under controlled storage, particularly in samples with higher copper content, highlighting strong copper-ethanol interactions. Post-reaction analysis also revealed copper phase transitions during photocatalytic CO_2 reduction (CO_2RR). In uncontrolled storage, Cu^0 oxidizes to CuO; however, photocatalysis promotes a shift to Cu_2O, driven by ethanol oxidation. Furthermore, leached copper reduction on SnO_2 in water suggests a potential light-induced synthesis route for Cu-based wide band gap semiconductors and supports Cu redox cycling on the catalyst. These results confirm that adsorbed ethanol acts as an electron donor, actively participating in the photocatalytic process. This study emphasizes the importance of accounting for synthesis-derived adsorbates to ensure accurate and reliable photocatalytic data.

1. Introduction

One of the main challenges of humankind is the mitigation of the anthropogenic CO_2. Since, this stable molecule needs high energy input for its conversion, catalytic routes are required to decrease the thermodynamic energy barrier to convert CO_2 into products.[1] Specifically, in the photocatalytic CO_2 reduction reaction (CO_2RR), there is an effortless research branch aiming to unveil the main interactions of the catalytic surface for fundamental studies. Based on the context of renewable energies, achieving wide spectrum absorbance and stable catalysts is very desirable,[2] which includes the combination of oxides for better performance.

Copper-based materials are among the most prospective applications for CO_2RR in the future. Recent papers of our group have demonstrated that TiO_2 and Nb_2O_5-supported Cu nanoparticles are more stable than freestanding CuO, which tends to react with CO_2 and form carbonates that poison the photocatalyst surfaces.[3–5] This increase in stability is associated to the heterostructure formation, promoting the separation of oxidation and reduction events in different materials, that is, CO_2 reduction occurs in Cu sites, while water oxidation in the supporting oxide. Thus, these findings indicates that Cu sites are the actual CO_2RR catalysts, while the semiconductor is responsible for the coupled oxidative reaction routes.

However, the lack of reproducibility in the recent literature on Cu-based photocatalysts with TiO_2[6–24] leads to doubtful conclusions about CO_2 conversion to CO, as seen in Table S1. Despite these results being based on different synthetic routes and variations of the photocatalytic setup, noteworthy, there is a lack of a standard or a benchmark value, revealed by the criteria of classifying *"good"* or *"prospective"* catalysts. Indeed, some results lie in the detection limit of the analytical equipment or might be influenced by extraneous residues, which are relevant even at very low levels due to the typical photocatalytic production yields.

Seeking better stability, we proposed SnO_2 as support (i.e., SnO_2/Cu photocatalyst) due to its steadiness to sintering and reduction,[25,26] implying in a good n-type charge separator. This catalyst yielded very similarly to TiO_2 and Nb_2O_5-supported Cu catalysts in terms of product yields, although our preliminary results indicated a high yield deviation between experiments performed in 30 days with different samples obtained from the same synthesis stored in air (Figure 1A). This strong variation in the results could be attributed to the spontaneous oxidation of copper species (Figure 1B) or adsorbates contaminations as observed elsewhere.[27]

Reliable results are as crucial as high-efficiency materials. Hence, it is important to consider that most soft-chemical synthesis pathways can result in residual hydrates and adsorbates, which may hinder or overestimate photocatalytic outcomes. In the latter case, these residues can act as sacrificial agents, providing electrons for the reduction reaction. It is important to

[a] G. D. Iga, J. A. Torres, J. L. Vieira
Department of Chemistry, Federal University of São Carlos (UFSCar), São Carlos, SP 13565–905, Brazil

[b] G. D. Iga, J. B. G. Filho, J. A. Torres, C. Ribeiro
Embrapa Instrumentation, Rua XV de Novembro, 1452, São Carlos, SP 13560–970, Brazil
E-mail: caue.ribeiro@embrapa.br

Supporting information for this article is available on the WWW under https://doi.org/10.1002/cctc.202500618

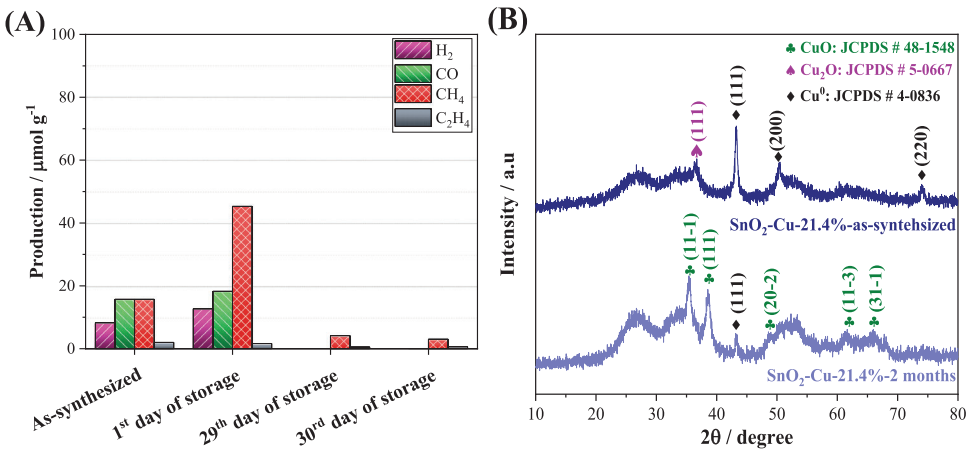

Figure 1. (A) Products in the headspace in function of the gap between reactions and (B) XRD diffraction of SnO_2/Cu-21.4 wt.% under uncontrolled storage conditions before and after 2 months. The synthesis follows the same procedure of this paper, as described in experimental methods.

highlight that, even in the event of contamination, these are still photocatalytic processes but driven by the oxidation of these extraneous species (instead of water oxidation). In this context, our hypothesis about these discrepancies is based on undesired reactions at the surface of the photocatalysts by species from synthesis methods, aging, or storage environments can promote. Sincethis can influence the production and properties of the photocatalysts, it is very important to understand how these factors can modify the nature of the photocatalytic sites.

Therefore, herein, we propose a detailed study of SnO_2/Cu photocatalyst activity for CO_2RR under different storage conditions and its evolution through time as a model to understand the indirect effects that can impact the photocatalytic results. The copper oxidation states were tracked by a variety of techniques, enabling the investigation of redox transitions and leaching in water. Moreover, the catalytic discrepancies were deeply discussed and supported the copper redox reversibility and its possible interaction with the synthesis adsorbates.

2. Experimental Section

2.1. Synthesis of SnO_2-3 h and SnO_2-10 h

The synthesis of SnO_2 nanoparticles was based on previous methodology,[28,29] consisting of the dissolution of 0.5 g of $SnCl_2.2H_2O$ (Aldrich) in 100 mL of anhydrous ethanol (99,5%, Êxodo) under vigorous magnetic stirring. Afterward, 24 mL of distilled H_2O was slowly added to the mixture and stirred for 24 h at room temperature. The resulting solid was washed with MILIQ H_2O and anhydrous ethanol by centrifugation until an $AgNO_3$ solution detected no chloride. The material was followed by a drying step in the oven at 50 °C and the particles were calcined in the muffle for 3 h or 10 h at 150 °C with a ramp rate of 10 °C min^{-1}. Importantly, the material calcined for 10 h was not washed with ethanol.

2.2. Synthesis of SnO_2/Cu and SnO_2/Cu-EtOH

The nanocrystalline SnO_2 particles were impregnated with copper as described by a previous method,[4] dispersing 1.0 g of this material in an ethanolic solution (10% v/v) in an ultrasonic bath for 10 min. The suspension was followed by a $Cu(NO_3)_2.3H_2O$ (Synth) addition in certain Cu mass proportions (calculated for 1.0, 10.0, or 30.0 wt.%:SnO_2 in the synthesis media) under vigorous stirring. After that, 100 mL of the reduction reagent $NaBH_4$ (Neon) was added to the suspension dropwise with its concentration proportional to the Cu loading (1 mol L^{-1} corresponds to 2.25 g of Cu). Lastly, the material was washed by centrifugation as it was described for pristine SnO_2, with or without ethanol (SnO_2/Cu-EtOH and SnO_2/Cu, respectively), frozen in liquid N_2, and dried under high vacuum for 48 h for its storage in an argon atmosphere. The effective Cu loadings in each catalyst was determined by chemical analysis (see below), considering losses during the sequential steps.

2.3. Characterization

The Cu loading and leaching were quantified by flame atomic absorption spectroscopy (FAAS) using a model PerkinElmer PinAAcle 900T spectrometer in 1% HNO_3 solutions. The crystalline phases were analyzed by X-ray diffraction before and after the reaction using the Shimadzu XRD 6000 instrument (2° min^{-1}, 10°–80° 2θ, Cukα = 1.5418 Å). A JEOL JEM-2100F and JEOL TECNAI G2 F20 electron transmission microscope (TEM) coupled to an energy-dispersive X-ray spectrophotometer (EDX) was applied to evaluate the copper dispersion. The nitrogen physisorption at −196 °C was obtained in a Micromeritics ASAP 2020, and the specific surface area (SSA) was calculated using the Brunauer–Emmett–Teller (BET) equation. Scattering electron microscopy (SEM) images were obtained using a JEOL microscope (JSM 6510) to analyze the particle shapes. Electron paramagnetic resonance (EPR) spectra were recorded on an X-band Bruker EMXplus spectrometer (MW frequency ∼ 9.78 GHz) and at room temperature and the g-factor values were obtained using the Bruker DPPH (2,2-diphenyl-1-picrylhydrazyl) standard as a reference. After the mass normalization, it was possible to track the relative concentration of Cu^{2+} species. Diffuse reflectance spectroscopy (DRS) was performed in Shimadzu UV-2600 to obtain the optical properties, specifically, the band-gap energy by the Kubelka–Munk theory.

2.4. CO_2 Reduction Reaction (CO_2RR)

All reactions were performed in a tubular quartz batch reactor with 100 mL of distilled water and 42 mL of headspace. Black tapes covered the gas phase region of the reactor to avoid irradiation that could promote photolysis. 15 min of high-purity CO_2 is bubbled until saturation and properly sealed with PTFE septum. The

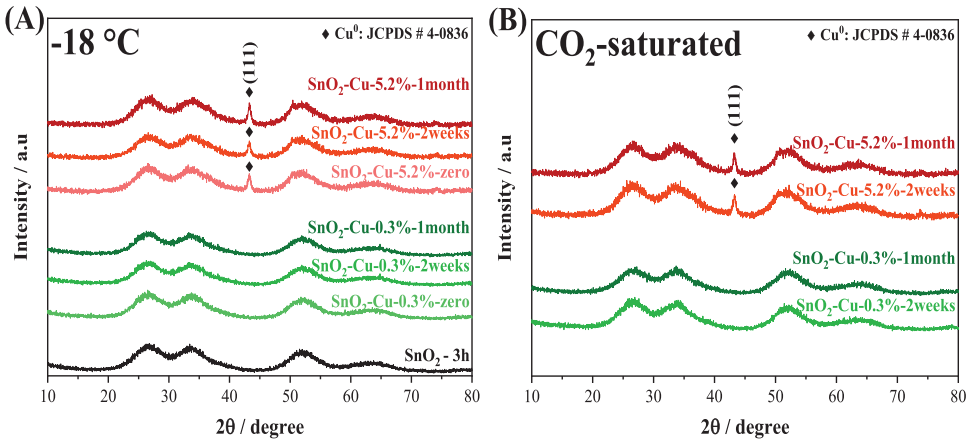

Figure 2. XRD in function of aging from (A) the photocatalysts stored at −18 °C and SnO_2 calcined for 3 h and (B) the materials stored in a CO_2-saturated environment.

reaction occurs in a refrigerated box with 6 UVC lamps (OSRAM, 15 W, 254 nm) calibrated with actinometric method. Every 2 h, the reactor's positions are randomly switched to keep the same statistical number of electrons received. The gas phase products were analyzed in the Agilent 8860 chromatograph equipped with an HP-Plot Q and Molsieve parallel column system, associated with an FID and TCD detector, respectively. The liquid phase was quantified by ^{1}H nuclear magnetic resonance (NMR) on a spectrometer of 600 MHz (Ascend 600 Bruker). For this, 540 µL of the sample was mixed with 60 µL of D2O and 2.24 mM of the reference 3-(trimethylsilyl)propionic-2,2,3,3-d4 acid sodium salt ($TSPd_4$). The water peak was suppressed, and NMR data were analyzed using the MestReNova software.

2.5. Storage Under Controlled Conditions

The as-synthesized photocatalysts were stored in two distinct environments to evaluate their stability over time. In a desiccator, 0.1 g of the materials were separated in opened Eppendorf's for further photocatalytic reaction and characterization. This desiccator was evacuated by a vacuum pump and filled with high-purity CO_2. Likewise, the 0.1 g of as-synthesized photocatalysts were stored in closed Eppendorf's and kept under −18 °C. The first reaction was entitled *"as-synthesized"*, and the subsequent materials were classified according to their storage environment and time. For example, CO_2 - 2 weeks.

3. Results and Discussion

3.1. Characterization

The photocatalysts were characterized by XRD to evaluate their bulk structure and a possible crystalline transition over time of storage under −18 °C and a CO_2-saturated environment (Figure 2A,B). All samples showed the expected nanocrystalline pattern of SnO_2 (JCPDS #41–1445), as has been shown in previous works.[28,29] The Cu^0 diffraction peak (JCPDS #4–0836) appeared as expected by the co-precipitation method,[4] except for the samples of lower Cu content. These samples did not change in function of time or distinct controlled storage environments, diverging from what was observed in an uncontrolled storage (Figure 1B). This evidence displays that the selected storage conditions were suitable to preserve the photocatalyst crystalline integrity, preventing a spontaneous phase transition. Nonetheless, the photocatalyst with 0.3 wt.% of Cu showed dispersed copper species from EDX analysis, justifying the absence of diffraction peaks by XRD (Figure S1).

The textural properties were investigated by nitrogen physisorption at 77 K (Figure 3A) and similar isotherm patterns were found, corresponding to the Type IV(a). There was a capillary condensation accompanied by hysteresis that typically occurs for materials with pores wider than ~4 nm,[30] exhibiting an H2 loop. This can be correlated to the small and inhomogeneous particles,[31] which were indeed identified by SEM microscopy for all photocatalysts (Figure 3B–E). Noteworthy, another hysteresis was observed for the Cu–5.2% at high relative pressures, which can be assigned to agglomerates that can mimic very large mesopores and macropores, although, its existence cannot be confirmed. Importantly, a broadening of capillary condensation compared to the pristine SnO_2 may be associated with the close packing between copper or tin nanoparticles,[31] increasing the relatively N_2 adsorbed quantity.

The Specific surface area (SSA) was calculated using the Brunauer–Emmett–Teller (BET) equation (Table 1). All materials presented a high surface area with similar values from multiple and reproducible nitrogen physisorption experiments, showing that the Cu content does not considerably affect the surface area. Conversely, these pore sizes or packing between the particles have comparable values, suggesting that the textural properties and the morphology of the materials were not significantly different to give insights of the aging effect of the catalysts.

3.2. Effect of the Storage Condition in CO_2RR

The spontaneous oxidation of an as-synthesized catalyst is highly undesirable feature of nanoparticles. This is a matter of great concern because only a few studies can track the photocatalyst change with the catalyst activity in experimental conditions. Therefore, two controlled storage environments were selected to

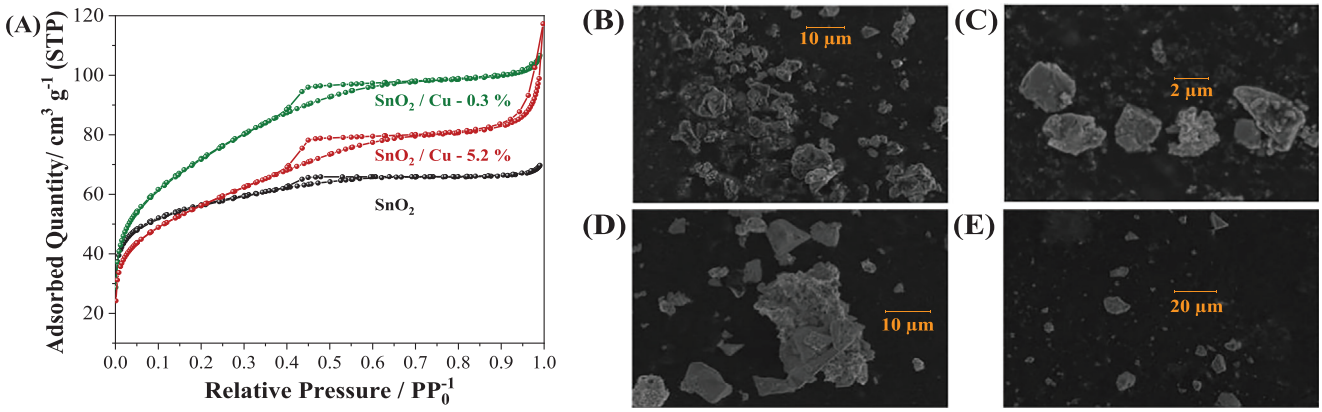

Figure 3. (A) Nitrogen physisorption isotherms obtained at 77 K. SEM images of photocatalysts with (B,C) 0.3%, (D) 5.2%, and (E) 21.4% of Cu loading.

Table 1. Textural and porous properties obtained by nitrogen physisorption at 77 K.s.

Sample	SSA_{BET}[a] ($m^2\ g^{-1}$)	V_{total} ($cm^3\ g^{-1}$)
SnO_2	210 (± 2)	0.1 (± 0)
SnO_2/Cu-0.3%	242 (± 12)	0.2 (± 0)
SnO_2/Cu-5.2%	194 (± 2)	0.1 (± 0)

[a] The partial pressure interval from 0.05 to 0.3 was used for the Cu-doped materials; and 0.01 to 0.05 for SnO_2, following the Rouquerol criteria.[32]

maintain the catalyst stability and track the catalyst changes over time.

In a CO_2-saturated storage environment, the photocatalyst surface can be saturated with the main reagent of the CO_2RR through adsorption.[33,34] Curiously, during one month of experiments, no activity loss was observed for gas phase products (Figure 4), in contrast to what was observed under an uncontrolled environment (Figure 1A). This photocatalytic behavior can be an indicator that the carbonatation of the surface may stabilize the active sites that lead to intermediates of gas phase products. Thus, CH_4 and CO were the main molecules detected for both photocatalysts, and with an increase in the copper load, a slightly higher productivity was observed, especially for H_2.

In the liquid phase (Figure 5), the detected species for the SnO_2/Cu-0.3% decreased significantly after the first reaction, suggesting that ethanol can be desorbed over time rather than a varied production of a photocatalyst that does not passes through a phase transition (Figure 2). However, as this tendency was not observed in the gas phase, the photocatalyst activity should be based on the gas phase products. Nevertheless, the deactivation trend was not replicated for SnO_2/Cu-5.2%, which has shown acetic acid as the main aqueous molecule. Despite the decrease in the first two weeks of storage, the experiment from the one-month stored material showed comparable production to the as-synthesized sample.

Another chosen method was the storage of the photocatalysts in low temperatures (−18 °C) to slow the kinetics of the surface reactivity. Under this condition, more materials were synthesized for a higher screening of the photocatalytic activity. The results of photocatalytic CO_2RR showed a comparable production pattern in function of the Cu content (Figure 6), regardless of the production variation per gram between each photocatalyst. Specifically, the gas phase tendency of the products was replicated in comparison of the CO_2-saturated environment, showing that both controlled environments warranted stability over time of storage.

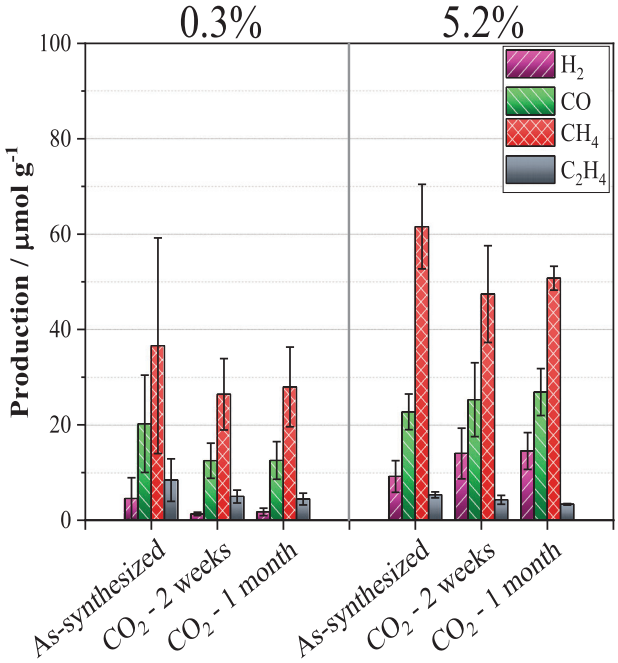

Figure 4. Products in the headspace obtained by CO_2 photoreduction of SnO_2/ Cu–0.3 and 5.2 wt.% in function of storage time in CO_2-saturated environment.

However, from the aqueous phase analysis, for 2 weeks, lower temperatures indeed prevented subtle evaporation of the synthesis adsorbates for the materials with less than 1 wt.% of Cu. This effect was not observed in the CO_2-saturated environment, which showed a higher decrease in the concentration of aqueous species at the same time of storage. Likewise, for the nanoparticles with a higher amount of copper, the aqueous phase products were shifted toward acetic acid. Hence, a

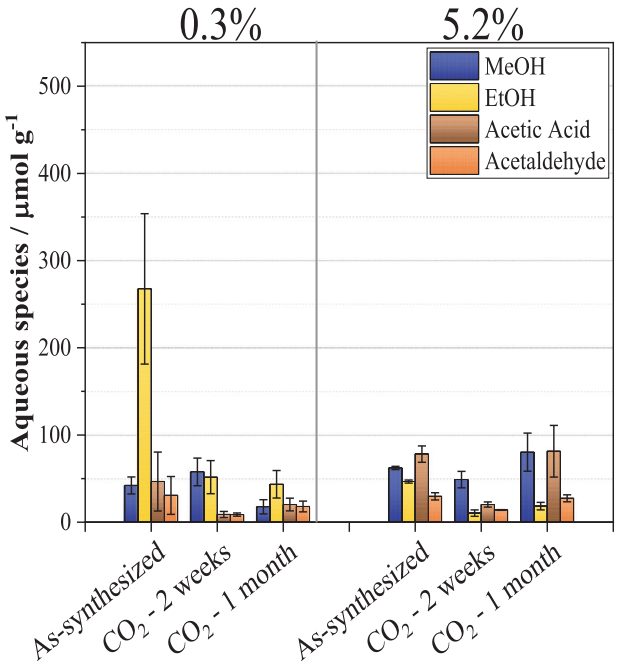

Figure 5. Aqueous molecules detected in the liquid phase obtained by CO_2 photoreduction of SnO_2/ Cu–0.3 and 5.2 wt.% in function of storage time in CO_2-saturated environment.

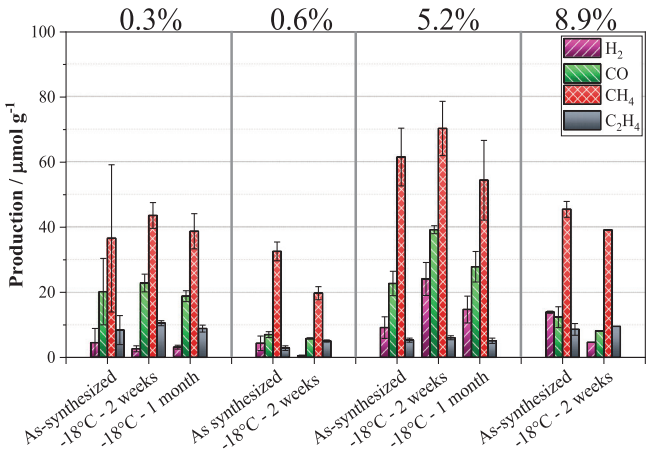

Figure 6. Products in the headspace obtained by CO_2 photoreduction of synthesized photocatalysts in function of storage time in −18 °C. Above the graphic, the Cu content for each batch of material.

higher amount of copper should stabilize the ethanol from the synthesis procedure, avoiding its evaporation in shorter periods of storage, and promoting its oxidation to acetic acid (Figure 7). This effect was observed in both controlled environments and with a wider range of Cu content, supporting this hypothesis.

Moreover, this strong binding with the photocatalytic surface and reproducible results can lead to erroneous interpretation of photocatalytic results. Additionally, the selectivity of many photocatalytic results[35–37] is often calculated by the rate of electrons involved in the formation of reduction products per mole of CO_2. However, acetaldehyde and acetic acid may be generated by oxidative routes instead of reduction ones, making this calculation unfeasible. Therefore, it is crucial to identify the effects of

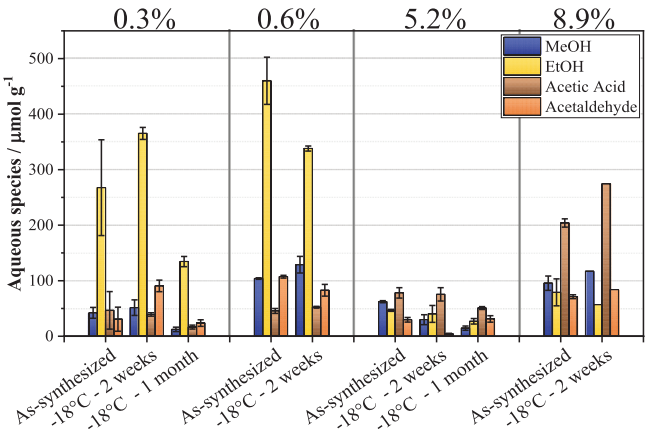

Figure 7. Aqueous molecules detected in the liquid phase obtained by CO_2 photoreduction of synthesized photocatalysts in function of storage time in −18 °C.

the residual adsorbates to ensure the development of reliable fundamental studies.

3.3. Role of Synthesis Components in Photoactivity

Sol-gel routes are popular due to the extreme versatility of products and have still been extensively used in different photocatalytic studies. On the other hand, the adsorption of counterions or solvents at surfaces can modify the activities since they can act as hole scavengers or as electrolytes, that is, changing the dynamics of charges. These adsorbates were identified in our synthesis, as seen in Figure S2, where one can see shifts related to the asymmetric bands of CH_3 and CH_2 vibrations at 2960 and 2920 cm^{-1}, respectively, and its overlap at 2850 cm^{-1}.[38] This band can be best related to solvents and synthesis inputs, and importantly, ethanol is essential for the nanocrystalline SnO_2 synthesis.[39] In addition, from the aqueous phase of each photocatalytic experiment of the previous section (Figures 5 and 7), this solvent should be the main carbonaceous adsorbate on the photocatalyst surface.

For the material with the lowest Cu content and the SnO_2 calcined for 3 or 10 h, this organic molecule vibration was superimposed by water and was not identified by FTIR. Thus, the investigation proceeded in the photocatalytic CO_2RR with pristine SnO_2 after the calcination at 150 °C for 3 h (Figure S3). The results have shown that ethanol was the molecule with higher concentration in the liquid phase, reaching values of 36.5 (± 3.4) µmol g^{-1}. In the gas phase, the CH_4 was quantified up to 15.5 (± 4.2) µmol g^{-1}. However, this wide band gap semiconductor is not reported as effective to dimerize the CO_2 to C_2 products in these experimental conditions. Indeed, the literature shows that the production of C_2 products using SnO_2-based materials is not likely to occur since the most common by-products are C_1 products, being C_2 minority.[28,29,40] In our experiments, it is noteworthy in this point that ethanol was the most common product. Thus, the detection of these relevant ethanol concentrations is a point of attention based in the information of the literature and should be investigated in deep.

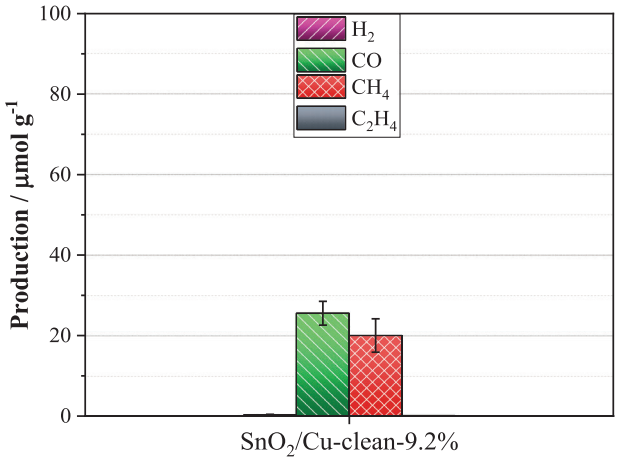

Figure 8. Production of the material without ethanol washing and 10 h of SnO_2 calcination at 150 °C.

To investigate the real activity of the material without an expressive concentration of carbonaceous species, the SnO_2 was re-synthesized and exhaustively washed with MILIQ water instead of ethanol. Additionally, this material was calcined at 150 °C for 10 h, and the Cu precipitation step also occurred with the absence of ethanol washing. This material was quantified with the 9.2 wt.% Cu and entitled as SnO_2/Cu-clean-9.2%. The results have shown only the production of CO and CH_4 (Figure 8), with no soluble byproducts detected by NMR. Therefore, the main photoactivity of SnO_2/Cu photocatalysts on CO_2RR is indeed the gas phase, and the products in the liquid phase were originated from the synthesis components. However, the production magnitude in the gas phase for the materials with synthesis adsorbates should not be overlooked, as the SnO_2/Cu-clean may not have the same population of hydroxyls on the surface, which, as previously reported, can impact the photocatalytic results.[28,29]

Furthermore, the synthesis residue was investigated by the argon-saturated reactions overnight to confirm any aqueous species that can be desorbed from the catalyst surface. The results showed no aqueous species for the sample with the absence of the ethanol washing step and the calcined SnO_2 for 10 h (SnO_2-10hcalc-Ar). The gas phase of this experiment revealed that there is a measurable CH_4 and CO production, which is, in this case, solely related to water as electron donor (Figure S4). This confirms the role of ethanol as electron donor in the enhanced photocatalytic activities, as proposed before. On the other hand, the samples with lower calcination time and ethanol washing (Figure S5) confirmed the ethanol adsorption from its oxidation products to acetate species (simplified to acetic acid, Equations 1–3).

$$H_2O \xrightarrow{h\nu} 2\,H_2 + O_2 \quad (1)$$

$$CH_3CH_2OH + \frac{1}{2}\,O_2 \rightarrow CH_3CHO + H_2O \quad (2)$$

$$CH_3CHO + \frac{1}{2}\,O_2 \rightarrow CH_3COOH \quad (3)$$

This issue was thoroughly discussed by Yang et.al., showing that the photocatalytic conversion of CO_2 and H_2O over TiO_2/Cu photocatalysts can be activated by carbon residues.[41] Thus, residual impurities in the reaction medium are a critical issue that must be identified as a priority in fundamental studies. Noteworthy, even the crystalline transition under an uncontrolled environment (Figure 1B) can relate to the interaction of surface adsorbates with copper. Therefore, for a better understanding of how this interaction should occur in a reaction environment, the post-reacted materials were evaluated to track Cu transitions after the reaction.

3.4. Analysis of the Materials Post-Reaction

The photocatalysts were centrifuged, dried in high vacuum, and further characterized post-reaction (PR). From the XRD analysis (Figure 9A,B), a phase transition from metallic Cu^0 (JCPDS # 4–0836) to the Cu_2O (JCPDS # 5–0667) was observed. This transition is highly desirable in the literature,[42–44] as Cu_2O is often correlated with the main active photocatalytic site for C—C the coupling reaction.

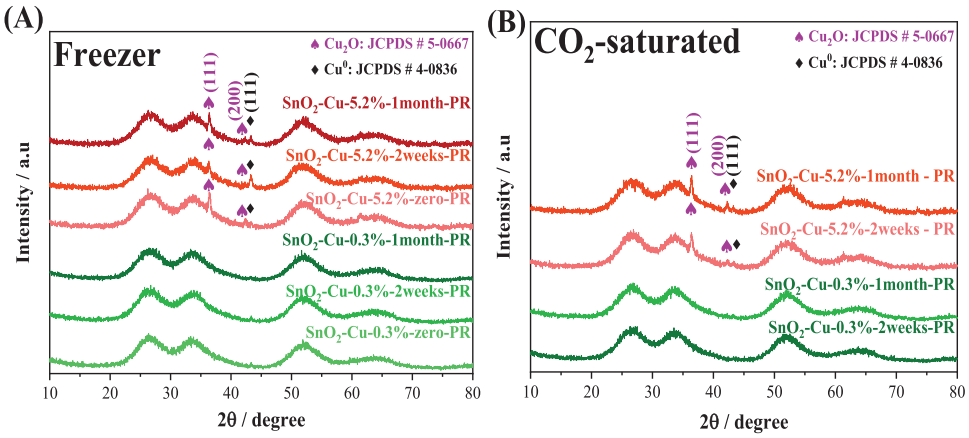

Figure 9. (A, B) XRD of the post-reacted photocatalysts.

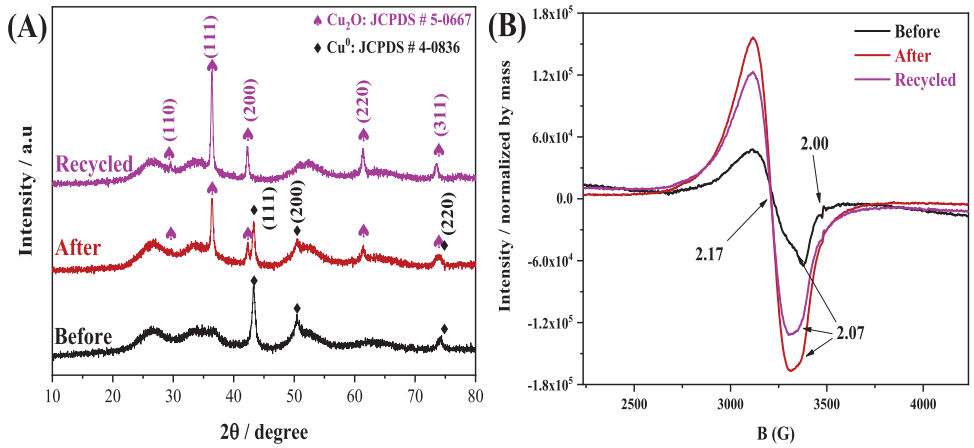

Figure 10. (A) XRD and (B) EPR spectra of SnO_2/Cu 21.4 wt.% photocatalysts, before and after reaction, and after recycling.

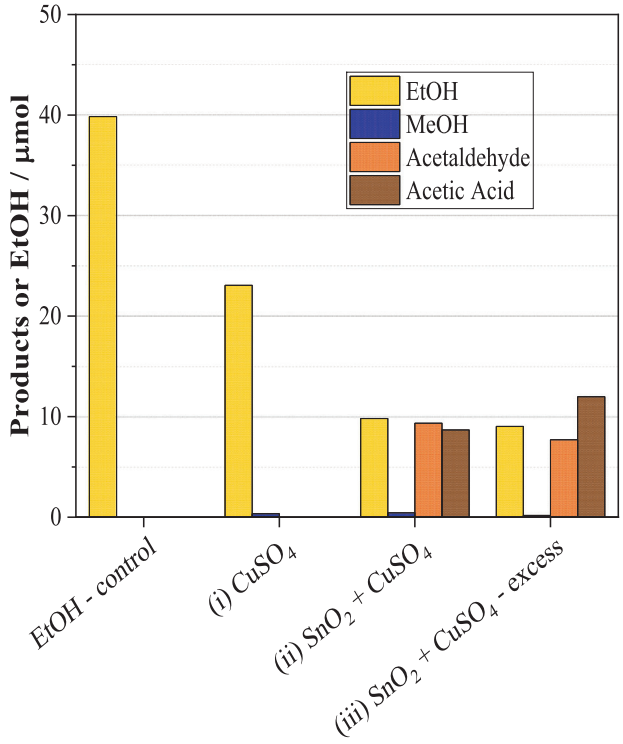

Figure 11. CO_2RR investigation with EtOH in the reaction medium. Tests were performed with $CuSO_4$ and SnO_2 + $CuSO_4$.

This Cu_2O transition was deeply investigated by XRD for a photocatalyst synthesized with a considerably higher amount of Cu content (Figure 10A). This photocatalyst transitioned to the Cu_2O phase until no metallic diffraction peaks appeared, suggesting that, while spontaneous deactivation under an uncontrolled environment favored the transition to CuO (Figure 1A), the photocatalytic reaction favored the Cu_2O phase.

Furthermore, to confirm the existence of the CuO, EPR experiments were conducted to track the paramagnetic centers of Cu^{2+} (Figure 10B). In comparison to the spectra before and after the reaction, this analysis revealed that Cu^{2+} (g-factor > 2.00, Table S3)[45,46] relative concentration considerably increased after the first reaction. However, after recycling, this paramagnetic center decreases, showing that these species are converted to another oxidation state (probably Cu^+ or Cu^0), following the tendency observed by XRD data. This phenomenon may be associated with copper redox reversibility ($Cu^0 \rightleftharpoons Cu^+ \rightleftharpoons Cu^{2+}$), as electrons are transferred to these species through the photocatalytic CO_2RR promoted by a UV source,[47] and it may be beneficial, increasing the lifetime of the h^+/e^- pair during the reaction.[48] Also, oxygen vacies (Ov) were detected in all of measured materials, which have the characteristic g-value of 2.00.[49]

Since, the pH of the reaction medium after the CO_2 saturation was experimentally determined to 4, the thermodynamic copper interactions with water should favors its ionization to Cu^{2+} as expressed by the Pourbaix diagram.[50] Previous studies by our research group discussed that the Cu^{2+} leaching occurs by the interaction with HCO_3^- species,[5,51] and the material changed to malachite ($CuCO_3.Cu(OH)_2$), in CO_2RR conducted in CO_2-saturated water. While this transformation occurred, the CO_2 was simultaneously converted during CuO carbonation process.[5] Hence, the duality of photocatalyst and reactant of Cu-based materials must be deeply investigated and will be explored in the next section.

3.5. The Role of the Copper Leaching

The aqueous samples after every reaction were analyzed by FAAS, and the copper leaching was quantified. The materials with the Cu 5.2 wt.% showed reproducible values (Table S2), and the percentage of leached copper was around 10.3%. The leaching in lower-content photocatalysts was below the technique limit for quantification.

Afterward, aiming to understand the interaction of the adsorbates with the aqueous environment, the reaction conditions were mimicked with the known parameters. For this, the reaction occurred in a solution containing 40 µmol of ethanol. Afterward, in a typical reaction system, three experiments were proposed to evaluate the role of Cu^{2+} in the CO_2RR: (i) the one with an expected concentration of leached copper (5.2 mg L^{-1}), but from

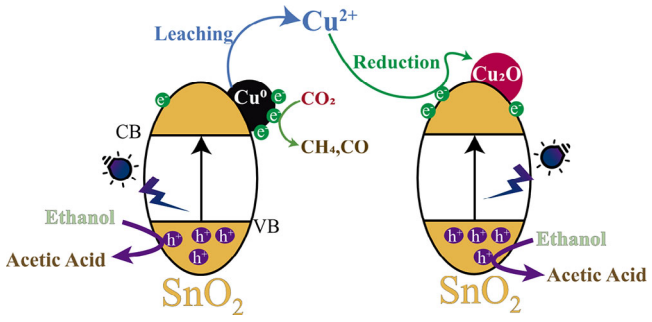

Figure 12. Mechanism proposed of the Cu_2O reprecipitation over SnO_2 during the CO_2RR.

$CuSO_4$, (ii) the same salt concentration with the addition of 0.1 g of SnO_2, and (iii) excess of $CuSO_4$ (20 mg L^{-1}) with the same amount of the SnO_2 (Figure 11).

The results in the gas phase with SnO_2 showed a comparable production presented in Figure S3, and the salt ethanolic solution showed no production. On the other hand, in the liquid phase (Figure 11), the results evidenced that UVC light with $CuSO_4$ favored the decomposition of ethanol to unidentified products, which could have been CO_2 and water. Nonetheless, in the presence of SnO_2, there was an oxidation of this synthesis component, which is also considered a hole scavenger, to acetaldehyde and acetic acid. Interestingly, the same products were observed in the liquid phase of SnO_2/Cu-5.2% and 8.9% (Figure 7), which may indicate the unavoidable copper leaching that promotes the further oxidation reactions.

Specifically, this oxidation step could occur with the interaction of Cu^{2+} and SnO_2, as this *n*-type semiconductor generates the electron/hole pair (e^-/h^+) by photoexcitation,[28,29] while ethanol acts as a reduction agent. Since no other products were observed, the reduction target could have been the Cu^{2+} ion, turning the crystalline phase to Cu_2O on SnO_2 by a reprecipitation process. This probable mechanism is illustrated in the Figure 12 below.

Importantly, similar photocatalytic results were obtained in the experiment with SnO_2 and an excess of $CuSO_4$, showing that the ethanol consumption is limited. However, the material changed its color considerably to reddish (Figure 13A). After the investigation by DRS analysis, it was possible to observe the band-gap of CuO and Cu_2O at 1.7 and 1.8 eV, respectively (Figure 13B). Noteworthy, there was a shift of the Cu_2O band gap to lower energies, which can facilitate the visible light absorption. Furthermore, EDX analysis confirmed highly dispersed Cu

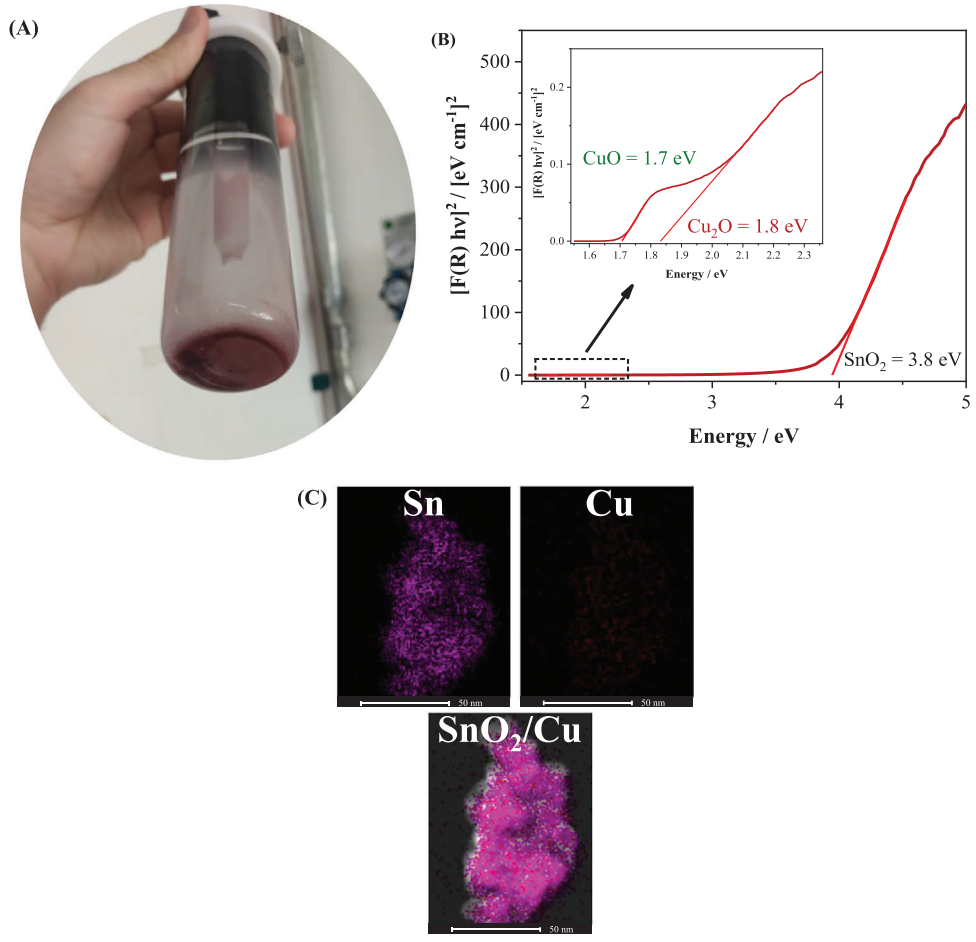

Figure 13. (A) Final color after CO_2RR with 20 mg L^{-1} of $CuSO_4$, EtOH (40 µmol) and 0.1 g of SnO_2. (B) DRS spectra of the resulting material, and an inlet graph corresponding to the zoomed area, showing the Cu species adhered in SnO_2. (C) EDX of this UV-induced synthesis of highly dispersed copper on SnO_2.

precipitation over SnO_2 by this UV-induced method with ethanol as a sacrificial agent (Figure 13C).

This kind of procedure is comparable to a synthesis with precipitation method assisted with ultrasound and microwave radiation,[52] which promoted the Cu_2O formation using glucose as a hole scavenger. Importantly, this kind of material has shown activity for water-splitting reactions and will be investigated in CO_2RR by future works.

In summary, the remaining ethanol from synthesis can lead to erroneous interpretation of photocatalytic results and instability of nanoparticles, acting as an electron donor for the photocatalytic process. Ethanol showed considerable stability and cannot be removed by conventional procedures, as frequently proposed by literature. On the other hand, it played a pivotal role in Cu redox reversibility over SnO_2. This result can lead to a light-induced synthesis methodology that can favor oxidative routes in other valuable chemicals and simultaneously promote the recyclability of the leached copper over wide band-gap semiconductors. Notwithstanding, the reproducibility of errors over well-controlled conditions must be warned to the scientific community for more reliable results in fundamental studies.

4. Conclusion

Herein, we proposed a fundamental study about SnO_2/Cu catalysts aiming to understand the effects of synthesis route and storage in the reliability of photocatalytic data. The results indicated that residual surface compounds from synthesis (e.g., ethanol) decisively influence the photocatalytic output by their oxidation, acting as a source of electrons for the whole photocatalytic process. These quantities are comparable to the commonly reported by related literature and are reproducibly seen in low temperatures of storage for two weeks. The ethanol stability can be related to a higher interaction strength of the ethanol with copper, although, further investigation is needed. This feature limits the catalytic performance validation and should be taken into consideration by the scientific community.

Furthermore, the post-reacted materials led to fundamental insights into the copper transition within the photocatalytic CO_2RR. While spontaneous oxidation to CuO occurs in an uncontrolled environment, after the photocatalytic reaction, Cu_2O transitions were observed. This transition was deeply investigated by tracking the copper species in the aqueous medium and using other characterization techniques. Control experiments showed evidence of the reduction of leached copper on SnO_2, which will be further investigated as a light-induced synthesis of Cu-based wide band gap semiconductors.

Author Contributions

Gustavo D Iga: Conceptualization; data curation; investigation; methodology; validation; writing—original draft. **José B. G. Filho**: Investigation; conceptualization; data curation; methodology. **Juliana A. Torres**: Investigation; conceptualization; methodology. **José Lucas Vieira**: Investigation. **Caue Ribeiro**: Conceptualization; supervision; funding acquisition; resources; writing—review & editing.

Acknowledgements

The authors acknowledge financial support from São Paulo Research Foundation (FAPESP) grant nos. #2022/07347–5, #2020/04109–0, #2023/10329–1, #2023/10329–1, and #2024/03871–7, and National Council for Scientific and Technological Development (CNPq) Projects 407878/2022–0, 4440117/2022-4, and 406925/2022-4 and grant nos. 382924/2023–1, 384762/2023–9, and 382687/2025-6. SISNANO/MCTI, FINEP (grant no. 01.24.0554.00), CAPES (Coordination for the Improvement of Higher Education Personnel-Finance Code 001), and the AgroNano Network (Embrapa Research Network) are also acknowledged. The authors also acknowledge the LNNano infrastructure for the additional EDX experiments (Proposal #20233520).

The Article Processing Charge for the publication of this research was funded by the Coordenacao de Aperfeicoamento de Pessoal de Nivel Superior - Brasil (CAPES) (ROR identifier: 00x0ma614).

Conflict of Interests

The authors declare no conflict of interest.

Data Availability Statement

Data available on request from the authors.

Keywords: CO_2 reduction · Copper · Ethanol · Photocatalysis · Stability

[1] X. Chang, T. Wang, J. Gong, *Energy Environ. Sci.* **2016**, *9*, 2177–2196.
[2] X. Chen, R. T. Guo, L. F. Hong, Y. Yuan, W. G. Pan, *Energy and Fuels* **2021**, *35*, 19920–19942.
[3] A. E. Nogueira, G. T. S. T. Silva, J. A. Oliveira, O. F. Lopes, J. A. Torres, M. Carmo, C. Ribeiro, *ACS Appl. Energy Mater.* **2020**, *3*, 7629–7636.
[4] J. A. Torres, J. C. da Cruz, A. E. Nogueira, G. T. S. T. da Silva, J. A. de Oliveira, C. Ribeiro, *J. Environ. Chem. Eng.* **2022**, *10*, 107291.
[5] A. E. Nogueira, G. T. S. T. da Silva, J. A. Oliveira, J. A. Torres, M. G. S. da Silva, M. Carmo, C. Ribeiro, *Catal. Commun.* **2020**, *137*, 105929.
[6] K. Zhu, Q. Zhu, M. Jiang, Y. Zhang, Z. Shao, Z. Geng, X. Wang, H. Zeng, X. Wu, W. Zhang, K. Huang, S. Feng, *Angew. Chem., Int. Ed.* **2022**, 61, https://doi.org/10.1002/anie.202207600.
[7] P. Chen, Z. Li, P. Wang, Y. Yao, T. Dou, Y. Qu, L. Jing, *Nanoscale* **2024**, *16*, 10727–10736.
[8] Z. Xiong, Z. Xu, Y. Li, L. Dong, J. Wang, J. Zhao, X. Chen, Y. Zhao, H. Zhao, J. Zhang, *Appl. Surf. Sci.* **2020**, *507*, 145095.
[9] N. Li, D. Geng, J. Zhou, *Catal Letters* **2022**, *152*, 124–138.
[10] M. Liu, X. Bao, F. Ma, M. Wang, L. Zheng, Z. Wang, P. Wang, Y. Liu, H. Cheng, Y. Dai, Y. Fan, Z. Zheng, B. Huang, *Chem. Eng. J.* **2022**, *429*, 132022.
[11] X. Bao, M. Zhang, Z. Wang, D. Dai, P. Wang, H. Cheng, Y. Liu, Z. Zheng, Y. Dai, B. Huang, *Chem. Eng. J.* **2022**, *445*, 136718.
[12] Z. Tai, G. Sun, T. Wang, Z. Li, J. Tai, *ACS Appl. Nano Mater.* **2022**, *5*, 18070–18079.

[13] Y. Shen, C. Ren, L. Zheng, X. Xu, R. Long, W. Zhang, Y. Yang, Y. Zhang, Y. Yao, H. Chi, J. Wang, Q. Shen, Y. Xiong, Z. Zou, Y. Zhou, *Nat. Commun.* **2023**, *14*, 1117.
[14] Z. Chen, L. Li, G. Cheng, *Carbon Lett.* **2023**, *33*, 1395–1406.
[15] H. Khan, R. C. Pawar, H. Charles, C. S. Lee, *Appl. Surf. Sci.* **2023**, *636*, 157832.
[16] B. Li, K. Zhang, X. Wang, Y. Li, X. Liu, B.-H. Han, F. Li, *J. Colloid Interface Sci.* **2024**, *660*, 961–973.
[17] A. A. Saraev, A. Yu Kurenkova, D. D. Mishchenko, A. L. Trigub, E. Yu Gerasimov, E. A. Kozlova, Transactions of Tianjin University **2024**, *30*, 140–151.
[18] M. Xu, C. Chen, X. Han, W. Hu, B. Li, *Colloids Surf. A Physicochem. Eng. Asp.* **2024**, *688*, 133676.
[19] A. Nishimura, H. Senoue, H. Mae, R. Hanyu, E. Hu, *Catalysts* **2024**, *14*, 270.
[20] Y. Cho, K. H. Kim, P. Dhak, Z. Wang, H. Jeong, H. Seo, K.-S. Lee, J. W. Han, S. H. Oh, J. H. Park, *ACS Energy Lett.* **2024**, *9*, 2739–2747.
[21] Y. Ru, Y. Chen, X. Yu, Q. Zhang, Y. Yin, G. Tian, *Sep. Purif. Technol.* **2024**, *349*, 127784.
[22] F. Yue, M. Shi, C. Li, Y. Meng, S. Zhang, L. Wang, Y. Song, J. Li, H. Zhang, *J. Colloid Interface Sci.* **2024**, *665*, 1079–1090.
[23] V. R. S. Nascimento, J. A. Torres, G. D. Iga, A. L. dos Santos, S. M. Egues, J. B. G. Filho, L. F. R. Ferreira, C. Ribeiro, *ChemCatChem* **2024**, *16*, https://doi.org/10.1002/cctc.202301612.
[24] C. Chen, T. Wang, K. Yan, S. Liu, Y. Zhao, B. Li, *Inorg. Chem. Front.* **2022**, *9*, 4753–4767.
[25] S. Fujihara, T. Maeda, H. Ohgi, E. Hosono, H. Imai, S. H. Kim, *Langmuir* **2004**, *20*, 6476–6481.
[26] R. Buckle, S. Roy, *Sep. Purif. Technol.* **2008**, *62*, 86–96.
[27] J. You, M. Xiao, S. Liu, H. Lu, P. Chen, Z. Jiang, W. Shangguan, Z. Wang, L. Wang, *J. Mater. Chem. A Mater.* **2023**, *11*, 10149–10154.
[28] J. A. Torres, G. T. S. T. Da Silva, F. Barbosa de Freitas Silva, C. Ribeiro, *ChemPhysChem* **2020**, *21*, 2392–2396.
[29] J. A. Torres, A. E. Nogueira, G. T. S. T. da Silva, C. Ribeiro, *ChemCatChem* **2023**, *15*, https://doi.org/10.1002/cctc.202201534.
[30] M. Thommes, K. Kaneko, A. V. Neimark, J. P. Olivier, F. Rodriguez-Reinoso, J. Rouquerol, K. S. W. Sing, *Pure Appl. Chem.* **2015**, *87*, 1051–1069.
[31] M. Dimitrov, T. Tsoncheva, S. Shao, R. Köhn, *Appl. Catal. B* **2010**, *94*, 158–165.
[32] J. Rouquerol, P. Llewellyn, F. Rouquerol, in *Characterization of Porous Solids VII, Studies in Surface Science and Catalysis*, Vol. *160*, (Eds: P. L. Llewellyn, F. Rodriquez-Reinoso, J. Rouqerol, N. Seaton), Elsevier, Amsterdam **2007**, pp. 49–56.
[33] W. Tu, Y. Zhou, Z. Zou, *Adv. Mater.* **2014**, *26*, 4607–4626.
[34] C. Genovese, C. Ampelli, S. Perathoner, G. Centi, *Green Chem.* **2017**, *19*, 2406–2415.
[35] P. Li, L. Liu, W. An, H. Wang, H. Guo, Y. Liang, W. Cui, *Appl. Catal. B* **2020**, *266*, 118618.
[36] S. Xie, Y. Wang, Q. Zhang, W. Deng, Y. Wang, *ACS Catal.* **2014**, *4*, 3644–3653.
[37] A. Raza, A. A. Haidry, Z. Yao, M. F. Saleem, A. A. Alothman, S. Mohammad, *Chem. Eng. J.* **2024**, *480*, 148162.
[38] T. Iwasita, E. Pastor, *Electrochim. Acta* **1994**, *39*, 531–537.
[39] C. Ribeiro, E. J. H. Lee, T. R. Giraldi, E. Longo, J. A. Varela, E. R. Leite, *J. Phys. Chem. B* **2004**, *108*, 15612–15617.
[40] Z. Guo, Y. Yu, C. Li, E. Campos dos Santos, T. Wang, H. Li, J. Xu, C. Liu, H. Li, *Angew. Chem., Int. Ed.* **2024**, *63*, https://doi.org/10.1002/anie.202319913.
[41] C. C. Yang, Y. H. Yu, B. Van Der Linden, J. C. S. Wu, G. Mul, *J. Am. Chem. Soc.* **2010**, *132*, 8398–8406.
[42] D. Zeng, H. Wang, X. Zhu, H. Cao, W. Wang, Y. Zhang, J. Wang, L. Zhang, W. Wang, *Appl. Catal. B* **2023**, *323*, 122177.
[43] W. Wang, C. Deng, S. Xie, Y. Li, W. Zhang, H. Sheng, C. Chen, J. Zhao, *J. Am. Chem. Soc.* **2021**, *143*, 2984–2993.
[44] L. Zhang, T. Liu, T. Liu, S. Hussain, Q. Li, J. Yang, *Chem. Eng. J.* **2023**, *463*, 142358.
[45] A. R. Fahami, T. Günter, D. E. Doronkin, M. Casapu, D. Zengel, T. H. Vuong, M. Simon, F. Breher, A. V. Kucherov, A. Brückner, J.-D. Grunwaldt, *React. Chem. Eng.* **2019**, *4*, 1000–1018.
[46] F. Wang, R. Büchel, A. Savitsky, M. Zalibera, D. Widmann, S. E. Pratsinis, W. Lubitz, F. Schüth, *ACS Catal.* **2016**, *6*, 3520–3530.
[47] T. H. Fleisch, G. J. Mains, *Appl. Surf. Sci.* **1982**, *10*, 51–62.
[48] L. Yuan, S. F. Hung, Z. R. Tang, H. M. Chen, Y. Xiong, Y. J. Xu, *ACS Catal.* **2019**, *9*, 4824–4833.
[49] K. Rahimi, A. Rawal, Y. F. Zhu, J. N. Hart, E. C. Lovell, J. Scott, *Appl. Catal. B Environ. Energy* **2024**, *359*, 124515.
[50] M. Spodaryk, K. Zhao, J. Zhang, E. Oveisi, A. Züttel, *Electrochim. Acta* **2019**, *297*, 55–60.
[51] A. E. Nogueira, J. A. Oliveira, G. T. S. T. da Silva, C. Ribeiro, *Sci. Rep.* **2019**, *9*, https://doi.org/10.1038/s41598-018-36683-8.
[52] E. Luévano-Hipólito, L. M. Torres-Martínez, D. Sánchez-Martínez, M. R. Alfaro Cruz, *Int. J. Hydrogen Energy* **2017**, *42*, 12997–13010.

Manuscript received: April 4, 2025
Revised manuscript received: May 23, 2025
Accepted manuscript online: May 24, 2025
Version of record online: ■■, ■■